Science of the Total Environment 839 (2022) 156149

Contents lists available at ScienceDirect

Science of the Total Environment

journal homepage: www.elsevier.com/locate/scitotenv

Effects of coal chemical industry on atmospheric volatile organic compounds emission and ozone formation in a northwestern Chinese city

Tianshu Chen [a], Liubin Huang [a,*], Xin Zhang [a,b], Rui Gao [b,*], Hong Li [b], Kai Fan [c], Dun Ma [c], Zhaokun Ma [d], Likun Xue [a,*], Wenxing Wang [a,b]

[a] Environment Research Institute, Shandong University, Qingdao 266237, China
[b] Chinese Research Academy of Environmental Sciences, Beijing 100012, China
[c] Yulin Municipal Ecology and Environment Bureau, Yulin 719000, China
[d] Shandong Academy for Environmental Planning, Ji'nan 250101, China

HIGHLIGHTS

- CCI contributed to 8.8 ± 1.8% of VOCs concentration, 17.9 ± 6.8% of OFP and 16.9 ± 7.4% of OH reactivity of VOCs.
- VOC compositions in Yulin were distinctly different to those in the megacities of China and typical oilfields worldwide.
- The concentration of naphthalene (1.6 ± 1.1 ppbv) in Yulin was greatly higher than that in other cities.
- VOCs emitted from CCI can promote O_3 production under snow cover resulted from the increased surface albedo.

GRAPHICAL ABSTRACT

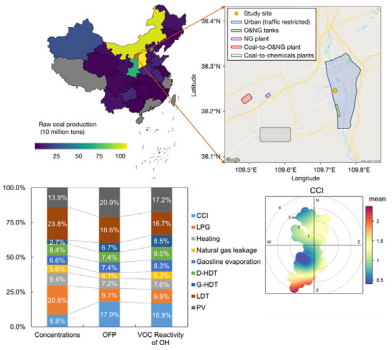

ARTICLE INFO

Editor: Hai Guo

Keywords:
Coal chemical industry
Volatile organic compounds
Ozone
Source apportionment
Photochemical process

ABSTRACT

Coal is well known as the primary energy consumption in China, and the coal chemical industry (CCI) can serve as an important source of volatile organic compounds (VOCs) emissions. However, the characteristics of VOCs emitted from CCI along with their environmental consequences are still poorly understood. To pin down this, an intensive field campaign was carried out at a typical CCI city in northwestern China (Yulin) from February 26 to March 7, 2021. Results showed that VOC compositions in Yulin were distinct from those in the megacities of China as well as in the typical oilfields over the world. The concentration of naphthalene (1.6 ± 1.1 ppbv), an important byproduct of CCI, was significantly higher than that in other cities (<0.2 ppbv). Positive matrix factorization (PMF) model analysis revealed that the direct contribution of the CCI source for VOC emissions is 8.8 ± 1.8%. More importantly, these VOCs emitted from the CCI can account for 17.9 ± 6.8% of ozone (O_3) formation potential and 16.9 ± 7.4% of OH reactivity of VOCs, suggesting the significant impacts of the CCI on the air quality and atmospheric oxidizing capacity. During the observation, a rapid increase in O_3 concentration after a snowfall was encountered. The changing rate of O_3 concentration in the daytime was significantly higher than in its peripheral cities. The increased O_3 formation was partially attributed to the CCI, and this enhancement can be further magnified by snow cover due to the increment of surface albedo. These findings deepen the understanding of the characteristics and air quality impact of VOCs related to the CCI and provide valuable insights for the development of air quality control measures in the region influenced by intensive coal chemical production.

* Corresponding authors.
E-mail addresses: hliubin@sdu.edu.cn (L. Huang), gaorui@craes.org.cn (R. Gao), xuelikun@sdu.edu.cn (L. Xue).

http://dx.doi.org/10.1016/j.scitotenv.2022.156149
Received 24 March 2022; Received in revised form 16 May 2022; Accepted 18 May 2022
Available online 26 May 2022

1. Introduction

As the Earth's population expands and the level of industrialization grows, human demand for energy (i.e., oil, natural gas, and coal) is unprecedented. The production and utilization of energy are commonly accompanied by the emission of pollutants (e.g., volatile organic compounds (VOCs) and nitrogen oxides (NO_x)) into the atmosphere, affecting the air quality and climate. Moreover, the oxidation of VOCs in the presence of NO_x can also produce secondary pollutants, such as ozone (O_3), inducing additional adverse effects on human health, ecology, and climate (Allen et al., 2013; Council, 1991; Edwards et al., 2014).

More than half of primary energy consumption worldwide comes from oil and natural gas (O&NG) (British Petroleum Company, 2021). Numerous studies have investigated the influences of O&NG activities on VOCs emission as well as O_3 formation (Abeleira et al., 2017; Ahmadov et al., 2015; Carter and Seinfeld, 2012; Chen et al., 2020; Field et al., 2015; McDuffie et al., 2016; Prenni et al., 2016; Schnell et al., 2009). For example, Edwards et al. (2014) reported that VOC concentration in the Uintah Basin (an oilfield in the U.S.) was ~15 times higher than in Los Angeles. The elevated VOC concentrations further generated more free radicals, resulting in pronounced O_3 production. McDuffie et al. (2016) highlighted that alkanes emitted from O&NG contribute approximately 20% to summertime regional photochemical O_3 production in the U.S. The model study revealed that O&NG production activities could make a dominant contribution to O_3 formation in those events through oxygenated VOC reactions (Edwards et al., 2014).

The characterizations of VOCs and their impacts on O_3 pollution in the typical O&NG areas in China have also been investigated. Chen et al. (2020) reported the highly abundant O&NG-related VOCs in the YelRD (Yellow River Delta) oilfield mainly composed of alkanes and aromatics. Those VOCs facilitated a stronger atmospheric oxidation capacity and rapid O_3 formation. However, compared to O&NG, it seems that coal plays a more significant role in the primary energy consumption in China. Statistical Review of World Energy pointed out that the fraction of coal (56.6%) in primary energy consumption is two times larger than that of O&NG (27.8%) (British Petroleum Company, 2021). The development of the coal chemical industry (CCI) not only acts as a supplement to O&NG but also provides raw materials for downstream chemical production (Xie et al., 2010). Future coal exploration and utilization may further increase in China due to the increasing energy demand. Therefore, it is essential to understand the impacts of coal exploration and utilization on VOCs and O_3 pollution what the latter is being the major air quality issue in China.

CCI can be divided into traditional CCI (e.g., coal coking, coal to ammonia, coal to urea) and modern CCI (e.g., coal to oil, coal to natural gas, coal to olefin) according to the maturity and history of the industry (Zhang et al., 2019a). VOC emission may be ubiquitous during CCI activities. Aries et al. (2007) found that aromatics were the dominant VOC group in the top of the coke oven and coal loading during coal coking processes. Li et al. (2018a) collected VOC samples from the top of coke ovens in the Beijing-Tianjin-Hebei region. They found that acetylene, benzene, ethane, and propane accounted for more than 86% of the VOCs emitted from the coal coking process. A recent study pointed out that 13% of industrial VOC emissions can come from coal coking in China in 2019 (Simayi et al., 2022). However, it is noted that previous studies about the amount and the characteristics of VOC emission from CCI were focused on specific processes such as coal coking (Simayi et al., 2022; Li et al., 2018a; Wu et al., 2016). Little is known about the role CCI plays in the VOCs pollution and O_3 formation on a local or urban scale in the atmosphere. Therefore, in this study, an intensive field campaign was conducted at Yulin, a typical CCI city in China, to explore the characteristics of VOCs emitted from the CCI and their effects on the wintertime O_3 formation. The detailed mechanism was further elucidated with the aid of an observation-constrained chemical box model. Furthermore, the characteristics of VOCs and O_3 in the coal city were also compared to typical O&NG production areas, aiming to provide new insights into the future formulation of specific air quality protection for different energy-industry-driven cities.

2. Materials and methods

2.1. Field experiments

Yulin is located north of Shaanxi Province, one of China's major coal production areas (Fig. 1a). It is a mid-level city (population of 3.41 million) in the south of the Hu-Bao-Er-Yu city cluster (Hohhot, Baotou, Ordos, and Yulin) – an important city cluster in northwest China. Compared with its adjoining cities, the CCI is more active in Yulin. Its raw coal and charcoal production accounted for 12.4% and 86.3% of their corresponding total production volumes in China in 2018, respectively (Yulin Daily, 2019). CCI areas are distributed in the southwest of Yulin (Fig. 1b). The field campaign was conducted on the top of the Environmental Monitoring

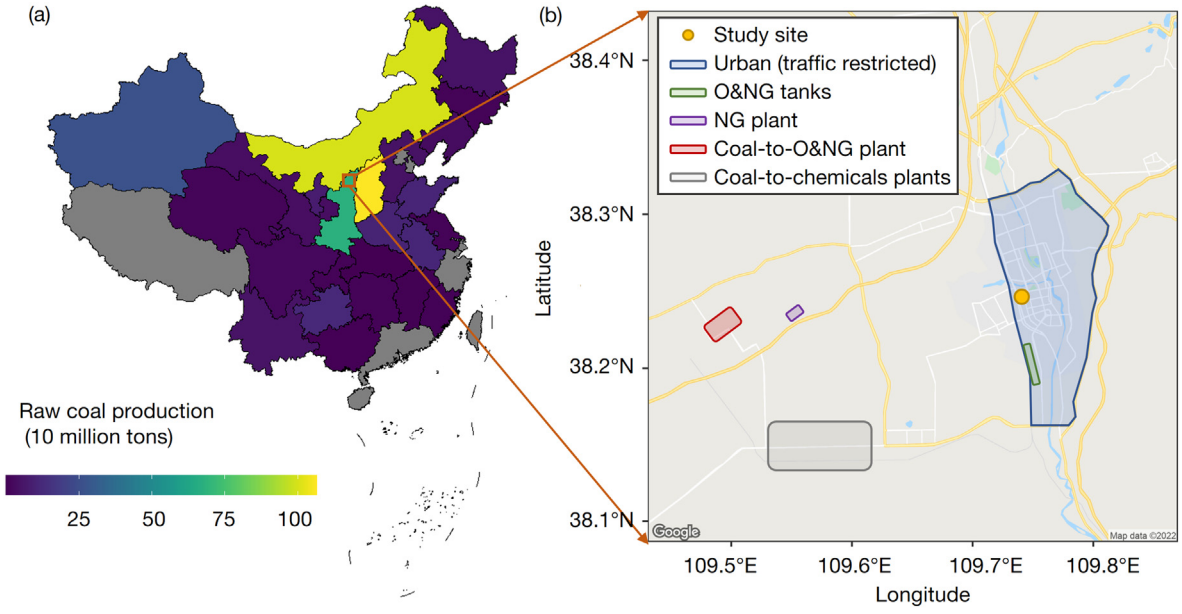

Fig. 1. Map showing (a) the raw coal production volumes in China in 2020 (the grey color presented no data, National Bureau of Statistics of China, 2021) and (b) the location of the study site and emission sources in Yulin.

Building (38.25°N, 109.73°E, 1095 m above sea level, 20 m above ground level) located on the west edge of the urban area and at the southwest of the CCI zone. During the observation period, the prevailing winds came from the southwest (Fig. S1). Thus, it is a suitable location to investigate the influence of the CCI on regional air quality. The field campaign was carried out from February 26 to March 7, 2021.

Air pollutants and meteorological parameters were measured by a series of commercial instruments during the campaign. O_3 was detected by an ultraviolet photometric analyzer (Thermo Environmental Instruments (TEI) model 49I). NO and NO_2 were measured by a chemiluminescent analyzer (TEI model 42I). CO was detected using a gas filter correlation nondispersive infrared analyzer (TEI model 48I). $PM_{2.5}$ was detected by a beta attenuation analyzer (TEI model 5028I). Meteorological parameters (including wind speed (WS), wind direction (WD), temperature (T), relative humidity (RH), and pressure (P) were measured by a weather station (LUFFT model WS-500). The resolution of instruments for air pollutants and meteorological parameters measurement is 1 min. The measured data were average and output from the data logger with a 5-mins resolution. Specifically, these data were averaged into a 1-h resolution for model input when modeling O_3 concentration. Table S1 shows the range, detection limit, and measurement frequency of the instruments used. Solar irradiances were measured by a radiation meter (Jinzhou Sunshine model TBQ-ZW-2). The range, detection limit, and measurement frequency of the instruments have been provided in Table S1. There was a snow process from midnight on February 28 to early morning on March 1. The thickness of the snow cover was 5 cm which was informed by the government notices. VOCs were measured at a one-hour resolution by online gas chromatography coupled with a mass spectrometer and a flame ionization detector (GC–MS/FID, AC-GCMS 1000, Hexin Instrument Co., Ltd). Ambient air samples were absorbed by two cold traps placed in the MS and FID sampling routes separately. After that, the samples were rapidly heated and evaporated at a rate of up to 50 °C s^{-1}, entering FID and MS for online qualitative and quantitative analysis. The instrument was calibrated by standard gas at 23:00 (UTC + 8) every day. Detailed information about the method of VOC detection and calibration can be seen in our previous study (Yin et al., 2021). A total of 77 VOCs (i.e., 29 alkanes, 11 alkenes, one ethyne, 17 aromatics, and 19 oxygenated VOCs) can be quantified. And these species were calibrated by standard gas, which is the mixture of PAMS and TO15. Note that oxygenated VOCs were only used as model input in this paper. Due to instrument maintenance, the VOC data were missed during February 26–28 and 10:00–23:00 on March 1. Details about the instrumental method have been listed in Table S2.

2.2. Positive matrix factorization model

The emission source profiles and their contributions to measured VOCs were calculated by the positive matrix factorization (PMF) model in version 5.0. The description of the model can be found in the EPA PMF 5.0 User Guide (Norris et al., 2014). PMF decomposes a specific sample matrix X into a source contribution matrix (G) and contaminant component spectrum matrix (F) according to observation data as shown in Eq. (1):

$$x_{ij} = \sum_{k=1}^{p} g_{ik} f_{kj} + e_{ij} \quad (1)$$

where x_{ij} is the concentration of the j species in the i sample; p is the number of sources; g_{ik} is the contribution of k source to the i sample, f_{kj} is the proportion of the j species in the k factor; e_{ij} is the residual of the j species in the i sample. The decomposing process requires the target function (Q) tends to be minimized (Eq. (2)):

$$Q = \sum_{i=1}^{n} \sum_{j=1}^{m} \left[\frac{x_{ij} - \sum_{k=1}^{p} g_{ik} f_{kj}}{u_{ij}} \right]^2 \quad (2)$$

where n and m represent the quantity of the sample and species, respectively. u_{ij} is the uncertainty of the j species in the i sample. The uncertainty of the j species can be expressed by either Eq. (3) or Eq. (4) based on the concentration of the j species.

$$\text{Uncertainty} = \frac{5}{6} \times \text{MDL} \quad (3)$$

$$\text{Uncertainty} = \sqrt{(\text{Error Fraction} \times \text{concentration})^2 + (0.5 \times \text{MDL})^2} \quad (4)$$

If the concentration was less than or equal to the method detection limits (MDL, see Table S2), the Eq. (3) was used, and otherwise, the Eq. (4) was used. The relative standard deviations (RSD) of VOCs were used as the error fractions (Table S2). RSD of specific VOC was calculated from the ratio of the average concentration of its standard gas (1 ppbv) to the corresponding standard deviation after seven times measurements. Selected VOC species were divided into three categories according to the signal-to-noise ratio (S/N) and percentages of value below the detection limit (BDL). Namely, the VOC species were classified as 'bad' if the S/N is <0.2 or the BDL percentage is >60.0%, as 'weak' if the S/N ranges from 0.2 to 2.0 or the BDL percentage is >50.0%, and as 'strong' if the S/N is >2.0 (Callén et al., 2014; Huang et al., 2015). The reasonableness of the identified results was estimated by the comprehensive consideration of two aspects: (1) Qrobust/Qexpected and (2) the physical plausibility of the factors(Chen et al., 2014; Huang et al., 2015). Qrobust is the goodness-of-fit parameter calculated excluding points that are not fit by the model. Qexpected is equal to (number of non-weak data values in X) minus (numbers of elements in G and F, taken together) (Norris et al., 2014):

$$Q_{exp} = (number\ of\ strong\ species \times number\ of\ samples) - \begin{pmatrix} (number\ of\ solution \times number\ of\ samples) + \\ (number\ of\ solution \times number\ of\ strong\ species) \end{pmatrix} \quad (5)$$

Lower Qrobust/Qexpected changing rate and lower Qrobust/Qexpected value indicate a better explanation of the model solution. In this study, solutions from five to ten factors were examined, and it was found that the changing rate of Qtrue/Qexpected with nine or ten factors was relatively low (Fig. S2). In addition, the solution of nine factors had the best physical plausibility. Thus, the solution of nine factors was eventually adopted in the present study.

2.3. O_3 formation potential and OH reactivity of VOCs

O_3 formation potential (OFP) has been widely used to quantify the relative impact of individual VOCs on O_3 formation (Zhang et al., 2021). The OFP can be calculated by multiplying concentration with maximum incremental reactivity (MIR) of individual VOCs. The values of MIRs for each species were obtained from the work of Zhang et al. (2021). Alternatively, for some species that were not included in Zhang's work, their values, as shown in Table S3, were obtained from the work of Carter (2009). The OH reactivity of VOCs is the loss frequency of OH defined as VOC concentration multiplied by its reaction rate coefficient with OH radical. The detailed reaction rate coefficient of each species (at 298 K) was accessed from the previous study (Atkinson and Arey, 2003).

2.4. Observation-based chemical box model

The Observation-Based Model for studying the Atmospheric Oxidation Capacity and Photochemistry (OBM-AOCP) was used to simulate the in situ atmospheric photochemical processes. The successful application of this model in previous studies has confirmed its reliability in simulating atmospheric chemical reactions (Li et al., 2018b; Sun et al., 2018; Xue et al., 2016; Yang et al., 2018). The latest version of the Master Chemical Mechanism (MCM v3.3.1) was used in this model. It is a nearly explicit mechanism describing the gas-phase chemical reactions that involve 143 primary VOC species (Saunders et al., 2003). O_3 production rate ($P(O_3)$)

is presented as the sum of reaction rates for HO_2 + NO and RO_2 + NO reactions, and O_3 loss rate ($L(O_3)$) is calculated as the sum of reaction rates for O_3 photolysis, O_3 + OH, O_3 + HO_2, O_3 + VOCs, NO_2 + OH, NO_2 + RO_2 (minus the decomposition rate of organic nitrates), NO_3 + VOCs, and loss of N_2O_5. The net O_3 production rate can be computed as the difference between $P(O_3)$ and $L(O_3)$. Note that the ozone production rates calculated by the box model usually correspond to the production of total oxidant (O_x = O_3 + NO_2) other than O_3 alone (Xue et al., 2013). Details about the O_3 chemistry calculation can be found in our previous studies (Xue et al., 2014; Xue et al., 2016).

Measured O_3, NO, NO_2, CO, and VOC concentrations, as well as meteorological data (relative humidity and temperature), were set as inputs of the model. VOC data was lacking from 10:00 to 23:00 (UTC + 8, same as below) on March 1 due to instrument maintenance. Considering the wind directions and wind speeds were similar between March 1 and 2, the missing VOC data on March 1 were supplied by the data from 10:00 to 23:00 on March 2, scaled by the ratio of VOCs averaged from 1:00 to 9:00 between those 2 days. The box model was run five times to stabilize unconstrained species. Only results from the last run were used for further analysis.

The Tropospheric Ultraviolet and Visible (TUV) Radiation Model was used to calculate the photolysis frequencies of NO_2 (J_{NO2}). Surface albedo and O_3 column density were used to constrain the TUV model. Since the snow depth changes over time were not available, in this study, the wet-bulb temperature was used to scale the snow depth over time. After that, the surface albedo of different snow depths was obtained by reviewing the plot of snow depth versus albedo in the literature (Perovich, 2007). The surface albedo was set as 0.10 when snow was melted. The average observed O_3 column density was obtained from the TROPOspheric Monitoring Instrument (TROPOMI). After the TUV model calculation, J_{NO2} was scaled by the ratio of the solar irradiance between measurement and the TUV model result. Scaled J_{NO2} was set as the input of the box model to constrain the photolysis frequencies of other species.

3. Results and discussions

3.1. Overview of filed observations

Fig. 2 shows the time series of meteorological parameters, NO_x (NO + NO_2), O_3, CO, and $PM_{2.5}$, during the campaign. The average concentrations (± standard deviation) of CO, NO_2, and NO were detected as 586.0 ± 255.0, 17.9 ± 11.6, and 10.3 ± 25.0 ppbv, respectively. It was found that CO was well correlated with NO_x (r^2 = 0.68, p < 0.05). The simultaneous increase of NO_x and CO was commonly observed in the nighttime. This is ascribed to the transportation of heavy-duty trucks (HDT) at night (Section 3.2). Accordingly, the slight peak of $PM_{2.5}$ that occurred in the nighttime may also be partially contributed by HDT. But haze event (defined by the 24 h-average $PM_{2.5}$ concentration exceeding 75.0 μg m^{-3}) was just encountered once throughout the ten-day observation period (March 7), and the average $PM_{2.5}$ concentration was measured as 38.3 ± 25.3 μg m^{-3}. The mean O_3 concentration was 28.4 ± 17.3 ppbv. O_3 concentration exhibited a dramatic diurnal variation. It decreased to almost zero during the night period due to the strong titration effect of NO, and then rapidly increased after sunrise with the peak and ~ 13:00 (UTC + 8). We also calculated the hourly changing rates of O_3, which is defined as the difference between the average O_3 concentration at a current hour and an hour after during the period of 8:00–14:00 (hereafter called daytime). The campaign-average changing rate was 4.5 ± 5.3 ppbv h^{-1}, with a maximum value of 23.9 ppbv h^{-1}. This value was higher than that in the peripheral cities of Yulin (3.3 ± 3.5 ppbv h^{-1} in Hohhot, 3.6 ± 3.0 ppbv h^{-1} in Baotou, 3.4 ± 3.6 ppbv

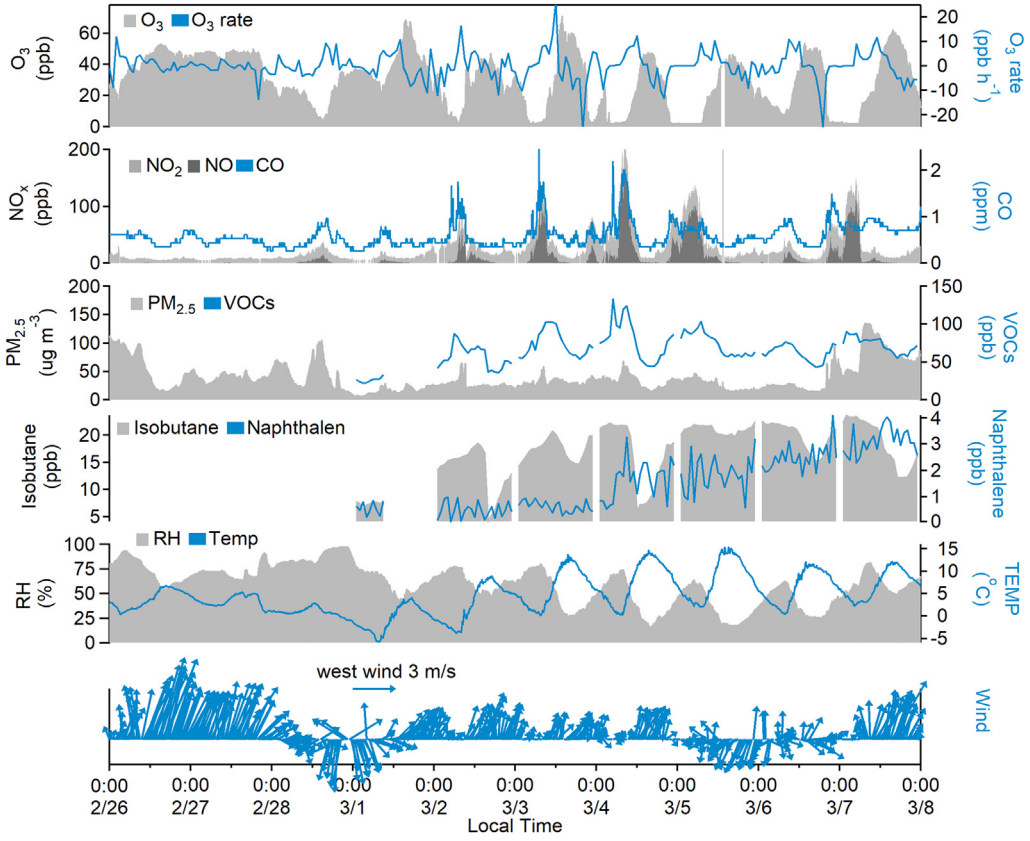

Fig. 2. Time series of meteorological parameters, O_3, NO_2, NO, CO, $PM_{2.5}$ concentrations, and O_3 changing rate in Yulin from February 26 to March 6, 2021.

Table 1
Comparison of VOCs average concentrations (contributions) in this study with other areas.

City	Alkanes	Alkenes	Alkyne	Aromatics	Total VOCs	Time period	Type	Reference
Yulin	43.5 (65.9%)	4.8 (6.6%)	9.2 (13.3%)	9.1 (14.2%)	66.7	2021.2.26–3.7	Urban	This study
Beijing	13.6 (54.8%)	1.9 (7.7%)	0.5 (2.0%)	8.8 (35.5%)	24.8	Spring of 2017	Urban	Zhang et al. (2020)
Guangzhou	20.2 (55.5%)	2.41 (6.6%)	1.71 (4.7%)	12.1 (33.2%)	36.4	2017.9.1–11.30	Urban	Meng et al. (2022)
Chengdu	29.2 (58.6%)	6.6 (13.3%)	8.5 (17.1%)	5.5 (11.0%)	49.8	2019.1.1–1.29	Urban	Xiong et al. (2021)
Wuhan	33.6 (63.0%)	6.6 (12.4%)	1.7 (3.2%)	11.4 (21.4%)	53.3	2017.1.22–2.21	Urban	Zheng et al. (2021)
Kuytun	21.2 (53.3%)	10.8 (27.1%)	5.4 (13.6%)	2.4 (6.0%)	39.8	2017.1.1–12.31	Near oilfield	Liang et al. (2020)
Dongying	22 (70.7%)	3.2 (10.3%)	2.9 (9.3%)	3 (9.6%)	31.1	2017.3.1–3.31	Near oilfield	Chen et al. (2020)
Boulder	42 (84.3%)	1.1 (2.2%)	1 (2.0%)	5.7 (11.4%)	49.8	2010.10.31–2011.3.18	Near oilfield	Field et al. (2015)
Denver	95.2 (97.4%)	0.9 (0.9%)	0.84 (0.9%)	0.8 (0.9%)	97.7	2011.2.18–3.7	Near oilfield	Gilman et al. (2013)

Noted: unit of all concentrations are ppbv.

h^{-1} in Ordos), indicating a more reactive O_3 formation in Yulin. The detailed mechanism for O_3 formation is discussed below.

The average concentration of VOCs was measured as 66.7 ± 20.1 ppbv during the whole campaign. In this study, VOCs measured were divided into four groups: alkanes, alkenes, alkyne, and aromatics. As shown in Table 1, alkanes were the dominant component in abundance, accounting for 65.9 ± 5.4% of total non-methane VOCs. Alkyne, alkenes, and aromatics accounted for 13.3 ± 5.5%, 6.6 ± 3.1%, and 14.2 ± 3.7%, respectively. It is found that a few species contribute to a large fraction of all VOC groups. For example, ethane, propane, butane, and pentane (C_2–C_5 alkanes) were the dominant compounds of alkanes (95.5 ± 1.1%); benzene, toluene, and naphthalene accounted for most of the aromatics (86.6 ± 3.4%). The concentrations of VOC species, as well as their corresponding fraction, are listed in Table S4. Isobutane was the most abundant VOC species (26.1 ± 5.6%), indicating a strong isobutane regional source in Yulin. Moreover, the ratio of isobutane to n-butane is calculated as 5.1 ± 0.3. Previous studies reported that the typical value of this ratio for raw natural gas and tank gas is lower than 1 (Roest and Schade, 2017). Given local industrial structures, the observed higher ratio may be attributed to liquefied petroleum gas usage. Another notable species is naphthalene, an important byproduct of the CCI (Price and Jayjock, 2008). The naphthalene concentration in Yulin (1.6 ± 1.1 ppbv) was much higher than normal ambient levels in other cities (<0.2 ppbv) (Jia and Batterman, 2010). These results suggest that detected VOCs may be mainly emitted from CCI and related activities.

Tables 1 and 2 summarize the concentrations of VOC compositions measured in the megacities of China and the oilfields over the world as a comparison. It is noted that the total VOC concentration in Yulin was 1.2–2.7 times higher than those measured in megacities (e.g., Beijing, Shanghai, Guangzhou, Chengdu, Wuhan), even though the population in these cities is at least 3.4 times larger than that in Yulin. Additionally, the major components of VOCs were also quite different. For example, the contribution of alkanes in Yulin was higher than in these megacities, and alkanes in urban areas typically originate from mobile sources rather than industrial activities. Alkyne, the tracer of combustion source, was also significantly higher in Yulin than in listed megacities except for Chengdu. But the contribution of aromatics, particularly for xylenes, in the megacities, was generally higher than that in Yulin. Xylenes were the species frequently found in Chinese cities and often have high loading in solvent usage sources (Hui et al., 2018; Ling et al., 2011; Zhang et al., 2020). The negligible concentration of xylenes (0.008 ± 0.003 ppbv) observed in Yulin during the campaign indicates a feeble influence of solvent sources. These results demonstrate the severe VOCs pollution and the pronounced characterization of VOCs components in Yulin arising from the CCI activities.

Furthermore, the concentration and compositions of VOCs were compared with those measured in oilfields. The concentration of VOCs in Denver is higher than that measured in Yulin. The possible explanation may be that the observation site was located in an area with a dense distribution of oil and gas wells in Denver (Gilman et al., 2013). Except for Denver, the total VOC concentration measured in Yulin was higher than in other oilfields, such as Kuytun, Dongying, and Boulder. Although alkanes were also the dominant VOCs in oilfields in analogous to Yulin, the primary components of alkanes are distinctly different. In Yulin, as mentioned above, isobutane was the most abundant alkane, but the dominant species in the oilfields are ethane and propane, the chemical reactivities of which were lower than that of isobutane. This discrepancy further highlights the difference in VOCs compositions between CCI and urban cities and oilfields, resulting in the difference in the mechanism for O_3 formation.

3.2. Importance of the coal chemical industry to ambient VOCs

The PMF model was employed further to quantify the contributions of different sources to the measured VOCs. A nine-factor resolution with a relatively lower Q value and the best plausibility of local industry and emission structures was obtained (see details in Methods, Fig. S2, and Fig. S3). Factor 1 was assigned to CCI because it can explain 74.2% of

Table 2
Comparison of top 10 VOC concentrations in this study with those in different areas.

City	Yulin	Bejing	Guangzhou	Chengdu	Wuhan	Kuytun	Dongying	Boulder	Denver
Isobutane	17.1	1.1	2.2	1.5	2.5	1.9	1.9	2.1	6.0
Acetylene	9.2	0.5	1.7	8.5	1.7	5.4	2.9	1.0	0.8
Ethane	8.4	1.9	2.4	10.4	7.0	5.4	6.4	23.2	35.0
Propane	8.3	2.3	4.6	6.5	9.9	4.0	6.3	8.9	27.0
n-Butane	4.9	1.9	3.9	2.5	7.2	2.3	3.2	2.3	14.0
Toluene	3.8	1.2	4.9	1.6	3.1	0.5	1.1	2.8	0.3
Ethylene	3.5	0.6	1.6	4.8	4.3	2.3	2.9	1.0	0.8
Benzene	2.5	5.4	0.7	1.3	3.8	0.7	1.1	1.0	0.3
Isopentane	2.0	0.7	2.3	1.3	2.9	2.4	1.7	1.3	4.2
Naphthalene	1.6	–	–	–	–	–	–	–	–
Period	2021.2.26–3.7	Spring of 2017	2017.9.1–11.30	2019.1.1–1.29	2017.1.22–2.21	2017.1.1–12.31	2017.3.1–3.31	2010.10.31–2011.3.18	2011.2.18–3.7
Type	Urban	Urban	Urban	Urban	Urban	Near oilfield	Near oilfield	Near oilfield	Near oilfield
Reference	This study	Zhang et al. (2020)	Meng et al. (2022)	Xiong et al. (2021)	Zheng et al. (2021)	Liang et al. (2020)	Chen et al. (2020)	Field et al. (2015)	Gilman et al. (2013)

Note: "–": no available data; unit of all concentrations: ppbv.

naphthalene, which has been identified as a high concentration in the emissions of the coal coking (Price and Jayjock, 2008). The more robust evidence is that Factor 1 showed high signal strength in the position of the coal-to-chemicals plants zone (Fig. 1 and Fig. 3A). Factor 2 was dominated by propane (45.6%), butanes (28.0%), and ethane (15.5%), which was majorly attributed to LPG emission (Chen et al., 2001; Liu et al., 2008). And the position of its high signal strength is close to the site (Fig. 3B). An oil/gas reservoir and a large oil/gas marketing company. Thus, Factor 2 was assigned to LPG eventually. Factor 3 was considered as heating based on the following consideration. Firstly, this factor is dominated by ethane (34.9%) and acetylene (26.5%) with poor correlation with other species, indicating contribution from natural gas combustion (Barletta et al., 2005; Li et al., 2014; Song et al., 2007). Secondly, the mean values of the daily factor strength from 09:00 to 23:00 had a very good negative correlation with temperature ($r^2 = 0.72$, $p < 0.01$), suggesting the contributions from heating. Thirdly, the strength of the factor signal appeared mainly to the southwest of the site, which was one of the main rural areas of Yulin (Fig. 3C). Natural gas burning has been one of the major clean heating ways in north China in recent years (Zhang et al., 2019b). Factor 4 was identified as gasoline evaporation since it has high loadings of $C_2 - C_5$ alkanes (68.3%) and can explain 52.5% and 47.0% of n-pentane and isopentane, respectively (Gilman et al., 2013). Factor 5 was characterized by the high content of ethane (69.5% of factor total). Ethane was the dominant compound in natural gas (Durana et al., 2006; Guo et al., 2011). This factor showed a higher signal in the northwest (Fig. 3E), where there was a large-scale natural gas processing plant (Fig. 1).

The remaining factors were closely related to traffic sources. Fig. 1b shows that the observation site is located at the edge of a restricted area and near the main traffic line. In the restricted area, heavy-duty trucks (mainly diesel vehicles) are prohibited from entering the restricted area in the whole day. Light-duty trucks cannot enter this area during off-peak commuting hours (1 h before and after commuting traffic).

As shown in Fig. 3F and G, the high strength of Factor 6 and Factor 7 is mainly concentrated around the intersection near the site. These two factors were assigned to the transportation of HDT, i.e., diesel-heavy duty truck (D-HDT) for factor 6 and gas-heavy duty truck (G-HDT) for Factor 7. G-HDT factor has a high proportion of propane (21.3%). Propane is the main component of LPG, the primary fuel for gas vehicles in this region (Wen, 2015). Diesel vehicles can emit higher concentrations of ethylene and acetylene than other vehicles, which is consistent with the source profile of D-HDT (Guo et al., 2011; Ling et al., 2011). Moreover, it is found that the VOC concentrations of these two factors were high in the early morning, when are the main driving hours for HDTs, supporting the results of factor assignments. The vehicle is the primary source of NOx and CO emissions in the atmosphere. The more robust evidence is that G-HDT and D-HDT factors have a strong correlation with NO ($r^2 = 0.68$, $p < 0.05$) and CO ($r^2 = 0.52$, $p < 0.1$) from 1:00 to 8:00, respectively

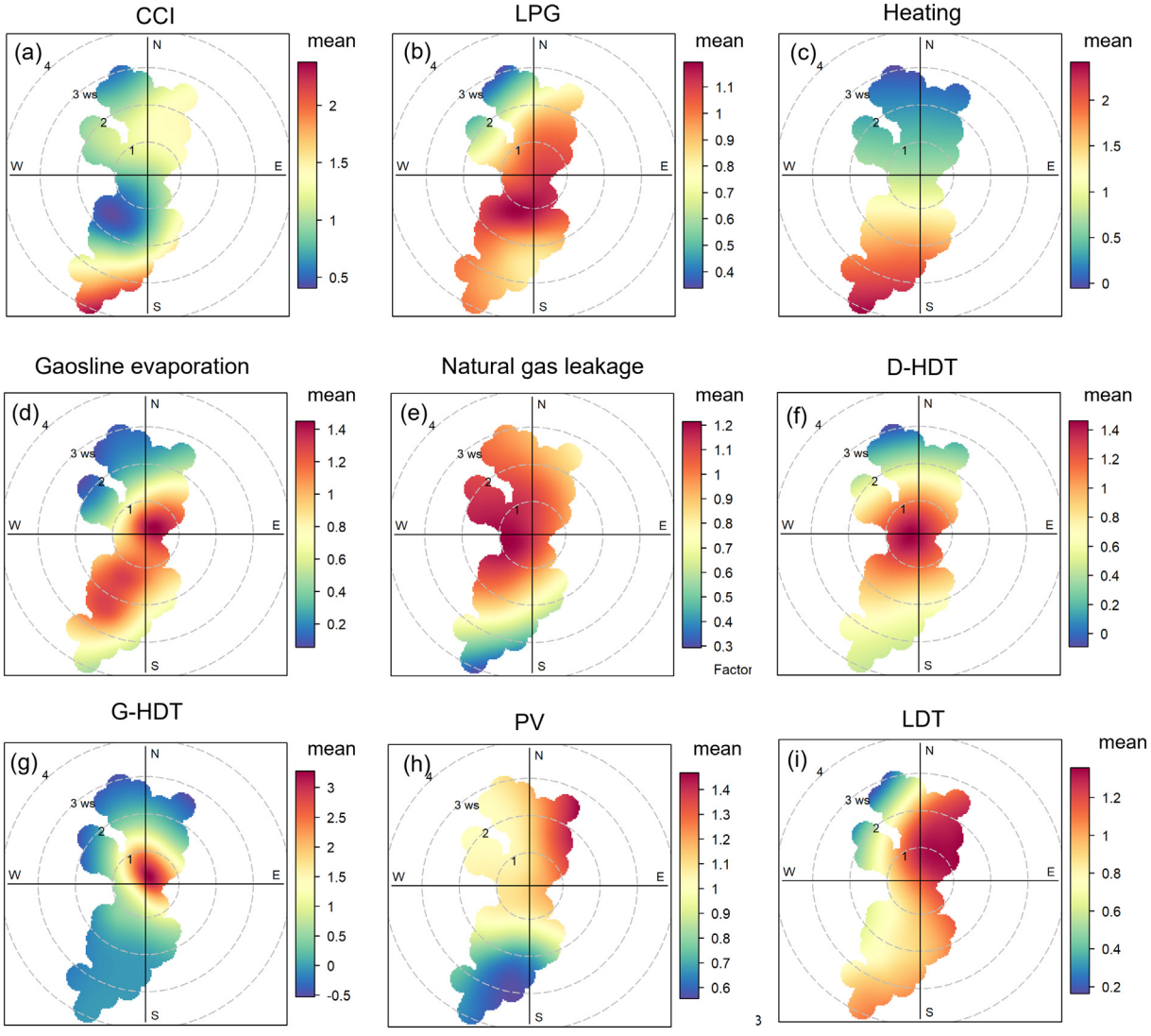

Fig. 3. Polar plot of the spatial distribution of the factor strength from February 26 to March 6, 2021.

(Fig. S4 and Fig. S5). Therefore, the increase in NOx and CO concentration is inferred to be attributed to the transportation of HDT in this study. In addition, the G-HDT factor shows a little loading of naphthalene which may attribute to local transportation for coal by HDTs.

Unlike the spatial distribution of the HDTs, the high strength of Factor 8 and Factor 9 are mainly located in the restricted traffic area, as shown in Fig. 3H and I. The ratios of benzene and toluene for Factor 8 and Factor 9 (0.4 and 0.7, respectively) are consistent with traffic sources (Barletta et al., 2005; He et al., 2015). The daily variations of these two factors display opposite trends during the peak commuting periods. Such characteristics of the two factors are consistent with the policy of controlling light-duty trucks (LDT) during the peak commuting period in the urban area. Factor 8 increases during the peak commuting period, and Factor 9 decreases during the peak period. In addition, Factor 8 intensity correlates better with octane. Generally, the passenger vehicle (PV) pursues a high compression ratio in the engine that requires gasoline with higher octane (Leone et al., 2015; Wu et al., 2019). Thus, Factor 8 and Factor 9 were considered PV and LDT, respectively. Both factors showed higher isobutane than other factors. It is considered that high concentrations of isobutane are mainly from gasoline emissions. The same conclusion was obtained from a recent study in Xi'an, a large neighboring city (Li et al., 2017).

Based on the source apportionment results, the contributions of different sources to VOC concentration during the campaign were further investigated. As shown in Fig. 4, the direction contribution for VOCs emission from CCI is 8.8 ± 1.8%. Vehicle sources (i.e., heavy-duty trucks, light-duty trucks, and passenger vehicles) were major contributors. Different types of traffic emissions accounted for 48.8 ± 3.7% of VOCs. Additionally, the contributions of VOCs emitted from different sources for OFP and OH reactivity of VOCs were also calculated. As shown in Fig. 4, VOCs directly emitted from various traffic sources contributed to 53.7 ± 5.4% of OFP and 51.9 ± 5.8% of OH reactivity of VOCs, which were similar to its contribution to the concentration of VOCs. However, the contributions of the CCI to OFP and OH reactivity of VOCs were different. The CCI had higher contributions to OFP (17.9 ± 6.8%) and OH reactivity of VOCs (16.9 ± 7.4%) than that to VOC concentration (8.8 ± 1.8%). Results show that naphthalene was the dominant contributor of CCI to OFP (65.7%) and OH reactivity of VOCs (70.5%). These results suggest the significant impacts of the CCI on the atmospheric oxidizing capacity. Moreover, the modern coal chemical industry in Yulin is entering a high-speed industrialization stage. CCI is expected to be playing a more vital role in the photochemical pollution in Yulin.

3.3. The mechanism for wintertime ozone formation in Yulin

VOCs are the major precursors for O_3 formation. As mentioned above, the changing rate of O_3 concentration during the whole campaign was a bit higher compared to its peripheral cities (Hu-Bao-Er-Yu city cluster),

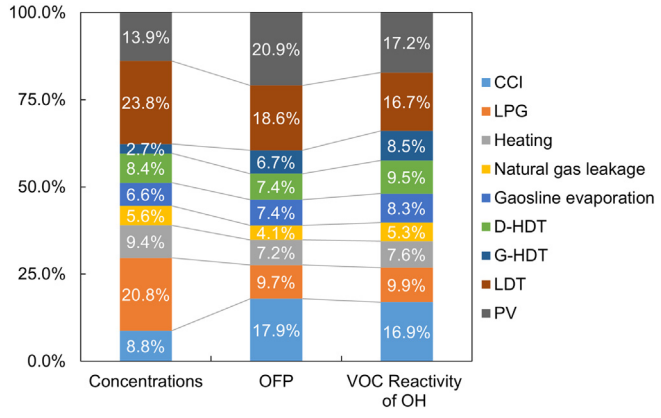

Fig. 4. Contribution of different sources to (a) VOC concentration, (b) O_3 formation potential, and (c) VOC reactivity of OH during the campaign.

where the CCI is less active, suggesting the potentially important role of CCI that plays in O_3 production. Moreover, it is interesting to find that the average hourly changing rate of O_3 in Yulin can be up to 3 times higher than the adjoining city cluster when the ground surface was covered by snow on March 1. The average O_3 concentration on this day (March 1, 43.5 ± 11.8 ppbv) was also higher than that before the snow (February 28, 11.4 ± 6.1 ppbv) and after the snow melted (March 2, 32.7 ± 7.7 ppbv) even though the NO_X concentration (11.2 ± 3.3 ppbv) and the meteorological conditions (T: 0.4 ± 2.2 °C) seem to be unfavorable for O_3 production. Previous studies reported that snow cover enhanced the surface albedo, thereby promoting the photolysis rate of radical precursors (Chen et al., 2020; Edwards et al., 2014). Therefore, field observation on March 1 was employed as the case to quantitively study the effects of CCI as well as snow cover on wintertime O_3 production.

A detailed chemical box modeling analysis was conducted to quantify the chemical budgets of O_3 production. The mechanism for O_3 production was simulated in three different scenarios (S1: without CCI and snow; S2: with CCI only; S3: with snow only; S4: with CCI and snow). The VOC concentrations ascribed to CCI by PMF were cut in scenarios S1 and S3. In the base simulation (scenario S1), the reaction of NO with HO_2 was the dominant pathway for O_3 formation (58.7 ± 3.2%) in the daytime, followed by the reaction of NO with RO_2 (40.1 ± 4.0%). The reaction of NO_2 with OH was the dominant removal pathway (47.5 ± 7.1%), followed by the reaction with NO_2 with RO (26.0 ± 8.6%).

The role of CCI-emitted VOCs plays in O_3 formation was then examined. It is noted that naphthalene related mechanism is lacking in the MCM v3.3.1. The overlook of naphthalene may result in the underestimation of O_3 production in Yulin, given the high concentration of naphthalene observed and its high MIR value calculated (8.9 mol mol^{-1}) (Carter, 2009). Since the MIR value of toluene (7.7 mol mol^{-1}) is close to naphthalene (Carter, 2009), and the OH reactivity of toluene and naphthalene both show a negative correlation with temperature, toluene was selected as the replacement of naphthalene to complement in the MCM v3.3.1 in this study and subsequently investigate the contribution of CCI to O_3 production. Adding VOC concentrations contributed by CCI into the model (S2) can promote 14.4% of the average O_3 net production rate and 16.8% of the maximum O_3 net production rate in the daytime (8:00–14:00).

However, the average rate during the same period in scenario S2 (3.2 ± 3.7 ppbv h^{-1}) is much lower than the average observation value (5.0 ± 2.9 ppbv h^{-1}). Thus, the effects of snow cover on March 1 were further assessed. Cater, and Seinfeld (Carter and Seinfeld, 2012) reported that the change in the surface albedo in snow cover could increase photolysis rates by a factor of 2.1 ± 0.3 on average. After considering the effects of snow cover (scenario S4), the average O_3 net production rate increased from 3.2 ± 3.7 ppbv h^{-1} to 5.0 ± 4.9 ppbv h^{-1}, and the maximum O_3 net production rate increased from 9.1 ppbv h^{-1} to 13.7 ppbv h^{-1}. The contributions of CCI under the effect of snow cover were assessed by the difference between S3 and S4. Overall, the model simulation results uncovered that VOCs emitted from CCI indeed enhance O_3 production, and this enhancement can be further magnified by snow cover due to the increment of surface albedo. Finally, it is worth noting that the observation was only carried out in winter in the present study, and it can be expected that the CCI-emitted VOCs may play a more significant role in the summertime ozone pollution under unfavorable conditions, which warrants more investigations in the future.

4. Conclusions

Intensive field observations and chemical box modeling were combined to understand the characteristics of VOCs and the O_3 formation mechanism in a CCI city (Yulin, China) in winter. C_2–C_5 alkanes, C_2–C_3 alkenes, acetylene, benzene, and toluene were the major compositions of VOCs measured. It is found that the VOC concentration in Yulin was higher than in the megacities in China and the typical oilfields over the world. In addition, compositions of VOCs were also distinctly different, suggesting

the severe VOCs pollution and obvious characterization of VOCs emission in the CCI city. Positive matrix factorization (PMF) model analysis revealed that the direct contribution of the CCI source for VOCs emission is 8.8 ± 1.8%, and these VOCs emitted from the CCI can account for 17.9 ± 6.8% of ozone (O_3) formation potential and 16.9 ± 7.4% of OH reactivity of VOCs, implying the significant impacts of the CCI on the air quality and atmospheric oxidizing capacity.

Furthermore, a detailed chemical box modeling analysis was conducted to understand the mechanism for O_3 formation in the CCI city. Results of model simulation uncovered that VOCs emitted from CCI indeed enhance O_3 production, and this enhancement can be further magnified by snow cover due to the increment of surface albedo. This study characterizes the unique chemical compositions of VOCs related to the CCI for the first time. It underlines the potential significance of CCI to ambient VOCs and O_3 pollution in coal industrial regions. Considering the large contribution of CCI to industrial VOC emission in China, clean energy and environment-friendly CCI technology are in high demand to improve regional air quality in similar energy-driven areas.

CRediT authorship contribution statement

Tianshu Chen: Methodology, Investigation, Writing – original draft. **Liubin Huang:** Writing – review & editing. **Xin Zhang:** Resources, Data curation. **Rui Gao:** Conceptualization, Resources, Data curation. **Hong Li:** Resources, Data curation. **Kai Fan:** Resources, Data curation. **Dun Ma:** Resources, Data curation. **Zhaokun Ma:** Resources, Data curation. **Likun Xue:** Conceptualization, Supervision, Resources, Writing – review & editing. **Wenxing Wang:** Supervision, Resources.

Declaration of competing interest

The authors declare that they have no known competing financial interests or personal relationships that could have appeared to influence the work reported in this paper.

Acknowledgments

The authors thank the University of Leeds for providing the MCM v3.3.1 and Glenn M. Wolfe for the Framework for 0-D Atmospheric Modeling (F0AM). The authors also thank Ning Li and Xiaolan Wang from Yulin Municipal Ecology and Environment Bureau for their help with VOC data processing. This study is funded by the National Natural Science Foundation of China (grant no. 41922051), the Shandong Provincial Science Fund for Distinguished Young Scholars (ZR2019JQ09), the Foundation for Qilu Young Scholar of Shandong University, and the Jiangsu Collaborative Innovation Center for Climate Change.

Appendix A. Supplementary data

Supplementary data to this article can be found online at https://doi.org/10.1016/j.scitotenv.2022.156149.

References

Abeleira, A., Pollack, I.B., Sive, B., Zhou, Y., Fischer, E.V., Farmer, D.K., 2017. Source characterization of volatile organic compounds in the Colorado northern front range metropolitan area during spring and summer 2015. J. Geophys. Res. Atmos. 122, 3595–3613. https://doi.org/10.1002/2016JD026227.

Ahmadov, R., McKeen, S., Trainer, M., Banta, R., Brewer, A., Brown, S., Edwards, P.M., de Gouw, J.A., Frost, G.J., Gilman, J., Helmig, D., Johnson, B., Karion, A., Koss, A., Langford, A., Lerner, B., Olson, J., Oltmans, S., Peischl, J., Pétron, G., Pichugina, Y., Roberts, J.M., Ryerson, T., Schnell, R., Senff, C., Sweeney, C., Thompson, C., Veres, P.R., Warneke, C., Wild, R., Williams, E.J., Yuan, B., Zamora, R., 2015. Understanding high wintertime ozone pollution events in an oil- and natural gas-producing region of the western US. Atmos. Chem. Phys. 15, 411–429. https://doi.org/10.5194/acp-15-411-2015.

Allen, D.T., Torres, V.M., Thomas, J., Sullivan, D.W., Harrison, M., Hendler, A., Herndon, S.C., Kolb, C.E., Fraser, M.P., Hill, A.D., Lamb, B.K., Miskimins, J., Sawyer, R.F., Seinfeld, J.H., 2013. Measurements of methane emissions at natural gas production sites in the United States. Proc. Natl. Acad. Sci. 110, 17768. https://doi.org/10.1073/pnas.1304880110.

Aries, E., Ciaparra, D., Schofield, M., Anderson, D., Schofield, N., Fisher, R., 2007. Fugitive and stationary source emissions from coke plants and impact on the local ambient air quality. Year-Book Coke Oven Manag. Assoc. UK, pp. 136–197.

Atkinson, R., Arey, J., 2003. Gas-phase tropospheric chemistry of biogenic volatile organic compounds: a review. Atmos. Environ. 37, 197–219.

Barletta, B., Meinardi, S., Sherwood Rowland, F., Chan, C.-Y., Wang, X., Zou, S., Yin Chan, L., Blake, D.R., 2005. Volatile organic compounds in 43 chinese cities. Atmos. Environ. 39, 5979–5990. https://doi.org/10.1016/j.atmosenv.2005.06.029.

British Petroleum Company, 2021. Statistical Review of World Energy. British Petroleum Company.

Callén, M.S., Iturmendi, A., López, J.M., 2014. Source apportionment of atmospheric PM2.5-bound polycyclic aromatic hydrocarbons by a PMF receptor model. Assessment of potential risk for human health. Environ. Pollut. 195, 167–177. https://doi.org/10.1016/j.envpol.2014.08.025.

Carter, W.P.L., 2009. Updated maximum incremental reactivity scale and hydrocarbon bin reactivities for regulatory applications. Calif. Air Resour. Board Contract 2009, p. 339.

Carter, W.P.L., Seinfeld, J.H., 2012. Winter ozone formation and VOC incremental reactivities in the upper Green River Basin of Wyoming. Atmos. Environ. 50, 255–266. https://doi.org/10.1016/j.atmosenv.2011.12.025.

Chen, T., Simpson, I.J., Blake, D.R., Rowland, F.S., 2001. Impact of the leakage of liquefied petroleum gas (LPG) on Santiago air quality. Geophys. Res. Lett. 28, 2193–2196.

Chen, T., Xue, L., Zheng, P., Zhang, Y., Liu, Y., Sun, J., Han, G., Li, H., Zhang, X., Li, Y., Li, H., Dong, C., Xu, F., Zhang, Q., Wang, W., 2020. Volatile organic compounds and ozone air pollution in an oil production region in northern China. Atmos. Chem. Phys. 20, 7069–7086. https://doi.org/10.5194/acp-20-7069-2020.

Chen, W.T., Shao, M., Lu, S.H., Wang, M., Zeng, L.M., Yuan, B., Liu, Y., 2014. Understanding primary and secondary sources of ambient carbonyl compounds in Beijing using the PMF model. Atmos. Chem. Phys. 14, 3047–3062. https://doi.org/10.5194/acp-14-3047-2014.

Council, N.R., 1991. Rethinking the Ozone Problem in Urban and Regional Air Pollution. The National Academies Press, Washington, DC. https://doi.org/10.17226/1889.

Durana, N., Navazo, M., Gómez, M.C., Alonso, L., García, J.A., Ilardia, J.L., Gangoiti, G., Iza, J., 2006. Long term hourly measurement of 62 non-methane hydrocarbons in an urban area: main results and contribution of non-traffic sources. Atmos. Environ. 40, 2860–2872. https://doi.org/10.1016/j.atmosenv.2006.01.005.

Edwards, P.M., Brown, S.S., Roberts, J.M., Ahmadov, R., Banta, R.M., deGouw, J.A., Dubé, W.P., Field, R.A., Flynn, J.H., Gilman, J.B., Graus, M., Helmig, D., Koss, A., Langford, A.O., Lefer, B.L., Lerner, B.M., Li, R., Li, S.-M., McKeen, S.A., Murphy, S.M., Parrish, D.D., Senff, C.J., Soltis, J., Stutz, J., Sweeney, C., Thompson, C.R., Trainer, M.K., Tsai, C., Veres, P.R., Washenfelder, R.A., Warneke, C., Wild, R.J., Young, C.J., Yuan, B., Zamora, R., 2014. High winter ozone pollution from carbonyl photolysis in an oil and gas basin. Nature 514, 351–354. https://doi.org/10.1038/nature13767.

Field, R.A., Soltis, J., McCarthy, M.C., Murphy, S., Montague, D.C., 2015. Influence of oil and gas field operations on spatial and temporal distributions of atmospheric non-methane hydrocarbons and their effect on ozone formation in winter. Atmos. Chem. Phys. 15, 3527–3542. https://doi.org/10.5194/acp-15-3527-2015.

Gilman, J.B., Lerner, B.M., Kuster, W.C., de Gouw, J.A., 2013. Source signature of volatile organic compounds from oil and natural gas operations in northeastern Colorado. Environ. Sci. Technol. 47, 1297–1305. https://doi.org/10.1021/es304119a.

Guo, H., Zou, S., Tsai, W., Chan, L., Blake, D., 2011. Emission characteristics of nonmethane hydrocarbons from private cars and taxis at different driving speeds in Hong Kong. Atmos. Environ. 45, 2711–2721.

He, Q., Yan, Y., Li, H., Zhang, Y., Chen, L., Wang, Y., 2015. Characteristics and reactivity of volatile organic compounds from non-coal emission sources in China. Atmos. Environ. 115, 153–162. https://doi.org/10.1016/j.atmosenv.2015.05.066.

Huang, Y., Ling, Z.H., Lee, S.C., Ho, S.S.H., Cao, J.J., Blake, D.R., Cheng, Y., Lai, S.C., Ho, K.F., Gao, Y., Cui, L., Louie, P.K.K., 2015. Characterization of volatile organic compounds at a roadside environment in Hong Kong: an investigation of influences after air pollution control strategies. Atmos. Environ. 122, 809–818. https://doi.org/10.1016/j.atmosenv.2015.09.036.

Hui, L., Liu, X., Tan, Q., Feng, M., An, J., Qu, Y., Zhang, Y., Jiang, M., 2018. Characteristics, source apportionment and contribution of VOCs to ozone formation in Wuhan, Central China. Atmos. Environ. 192, 55–71. https://doi.org/10.1016/j.atmosenv.2018.08.042.

Jia, C., Batterman, S., 2010. A critical review of naphthalene sources and exposures relevant to indoor and outdoor air. Int. J. Environ. Res. Public Health 7, 2903–2939. https://doi.org/10.3390/ijerph7072903.

Leone, T.G., Anderson, J.E., Davis, R.S., Iqbal, A., Reese, R.A., Shelby, M.H., Studzinski, W.M., 2015. The effect of compression ratio, fuel octane rating, and ethanol content on spark-ignition engine efficiency. Environ. Sci. Technol. 49, 10778–10789. https://doi.org/10.1021/acs.est.5b01420.

Li, B., Ho, S.S.H., Xue, Y., Huang, Y., Wang, L., Cheng, Y., Dai, W., Zhong, H., Cao, J., Lee, S., 2017. Characterizations of volatile organic compounds (VOCs) from vehicular emissions at roadside environment: the first comprehensive study in northwestern China. Atmos. Environ. 161, 1–12. https://doi.org/10.1016/j.atmosenv.2017.04.029.

Li, G., Wei, W., Shao, X., Nie, L., Wang, H., Yan, X., Zhang, R., 2018a. A comprehensive classification method for VOC emission sources to tackle air pollution based on VOC species reactivity and emission amounts. J. Environ. Sci. 67, 78–88. https://doi.org/10.1016/j.jes.2017.08.003.

Li, L., Chen, Y., Zeng, L., Shao, M., Xie, S., Chen, W., Lu, S., Wu, Y., Cao, W., 2014. Biomass burning contribution to ambient volatile organic compounds (VOCs) in the Chengdu-Chongqing region (CCR), China. Atmos. Environ. 99, 403–410. https://doi.org/10.1016/j.atmosenv.2014.09.067.

Li, Z., Xue, L., Yang, X., Zha, Q., Tham, Y.J., Yan, C., Louie, P.K.K., Luk, C.W.Y., Wang, T., Wang, W., 2018. Oxidizing capacity of the rural atmosphere in Hong Kong, Southern

China. Sci. Total Environ. 612, 1114–1122. https://doi.org/10.1016/j.scitotenv.2017.08.310.
Liang, Y., Liu, X., Wu, F., Guo, Y., Fan, X., Xiao, H., 2020. The year-round variations of VOC mixing ratios and their sources in Kuytun City (northwestern China), near oilfields. Atmos. Pollut. Res. 11, 1513–1523. https://doi.org/10.1016/j.apr.2020.05.022.
Ling, Z.H., Guo, H., Cheng, H.R., Yu, Y.F., 2011. Sources of ambient volatile organic compounds and their contributions to photochemical ozone formation at a site in the Pearl River Delta, southern China. Environ. Pollut. 159, 2310–2319. https://doi.org/10.1016/j.envpol.2011.05.001 Nitrogen Deposition, Critical Loads and Biodiversity.
Liu, Y., Shao, M., Fu, L., Lu, S., Zeng, L., Tang, D., 2008. Source profiles of volatile organic compounds (VOCs) measured in China: Part I. Atmos. Environ. 42, 6247–6260. https://doi.org/10.1016/j.atmosenv.2008.01.070 PRIDE-PRD 2004 Campaign: Program of Regional Integrated Experiments on Air Quality over Pearl River Delta of China.
McDuffie, E.E., Edwards, P.M., Gilman, J.B., Lerner, B.M., Dubé, W.P., Trainer, M., Wolfe, D.E., Angevine, W.M., deGouw, J., Williams, E.J., Tevlin, A.G., Murphy, J.G., Fischer, E.V., McKeen, S., Ryerson, T.B., Peischl, J., Holloway, J.S., Aikin, K., Langford, A.O., Senff, C.J., Alvarez II, R.J., Hall, S.R., Ullmann, K., Lantz, K.O., Brown, S.S., 2016. Influence of oil and gas emissions on summertime ozone in the Colorado northern front range. J. Geophys. Res. Atmos. 121, 8712–8729. https://doi.org/10.1002/2016JD025265.
Meng, Y., Song, J., Zeng, L., Zhang, Y., Zhao, Y., Liu, X., Guo, H., Zhong, L., Ou, Y., Zhou, Y., Zhang, T., Yue, D., Lai, S., 2022. Ambient volatile organic compounds at a receptor site in the Pearl River Delta region: variations, source apportionment and effects on ozone formation. J. Environ. Sci. 111, 104–117. https://doi.org/10.1016/j.jes.2021.02.024.
National Bureau of Statistics of China, 2021. The raw coal production volumes in China in 2020 ranked by provinces and regions [WWW Document]. URL https://www.china5e.com/news/news-1108480-1.html. (Accessed 28 May 2022).
Norris, G., Duvall, R., Brown, S., Bai, S., 2014. EPA Positive Matrix Factorization (PMF) 5.0 Fundamentals and User Guide.
Perovich, D.K., 2007. Light reflection and transmission by a temperate snow cover. J. Glaciol. 53, 201–210. https://doi.org/10.3189/172756507782202919.
Prenni, A.J., Day, D.E., Evanoski-Cole, A.R., Sive, B.C., Hecobian, A., Zhou, Y., Gebhart, K.A., Hand, J.L., Sullivan, A.P., Li, Y., Schurman, M.I., Desyaterik, Y., Malm, W.C., Collett Jr., J.L., Schichtel, B.A., 2016. Oil and gas impacts on air quality in federal lands in the bakken region: an overview of the bakken air quality study and first results. Atmos. Chem. Phys. 16, 1401–1416. https://doi.org/10.5194/acp-16-1401-2016.
Price, P.S., Jayjock, M.A., 2008. Available data on naphthalene exposures: strengths and limitations. Regul. Toxicol. Pharmacol. 51, 15–21. https://doi.org/10.1016/j.yrtph.2007.10.010 Supplement: Naphthalene State of the Science Symposium.
Roest, G., Schade, G., 2017. Quantifying alkane emissions in the eagle ford shale using boundary layer enhancement. Atmos. Chem. Phys. 17, 11163–11176. https://doi.org/10.5194/acp-17-11163-2017.
Saunders, S.M., Jenkin, M.E., Derwent, R.G., Pilling, M.J., 2003. Protocol for the development of the master chemical mechanism, MCM v3 (Part A): tropospheric degradation of non-aromatic volatile organic compounds. Atmos. Chem. Phys. 3, 161–180. https://doi.org/10.5194/acp-3-161-2003.
Schnell, R.C., Oltmans, S.J., Neely, R.R., Endres, M.S., Molenar, J.V., White, A.B., 2009. Rapid photochemical production of ozone at high concentrations in a rural site during winter. Nat. Geosci. 2, 120–122. https://doi.org/10.1038/ngeo415.
Simayi, M., Shi, Y., Xi, Z., Ren, J., Hini, G., Xie, S., 2022. Emission trends of industrial VOCs in China since the clean air action and future reduction perspectives. Sci. Total Environ. 826, 153994. https://doi.org/10.1016/j.scitotenv.2022.153994.
Song, Y., Shao, M., Liu, Y., Lu, S., Kuster, W., Goldan, P., Xie, S., 2007. Source apportionment of ambient volatile organic compounds in Beijing. Environ. Sci. Technol. 41, 4348–4353. https://doi.org/10.1021/es0625982.
Sun, J., Li, Z., Xue, L., Wang, T., Wang, X., Gao, J., Nie, W., Simpson, I.J., Gao, R., Blake, D.R., Chai, F., Wang, W., 2018. Summertime C1–C5 alkyl nitrates over Beijing, northern China: spatial distribution, regional transport, and formation mechanisms. Atmos. Res. 204, 102–109. https://doi.org/10.1016/j.atmosres.2018.01.014.
Wen, W., 2015. The Influence of Using Motor Vehicle Alternative Fuel (Natural Gas) on PM2.5 in Guanzhong Region And Abatement Analysis. Chang'an University (Master).
Wu, R., Bo, Y., Li, J., Li, L., Li, Y., Xie, S., 2016. Method to establish the emission inventory of anthropogenic volatile organic compounds in China and its application in the period 2008–2012. Atmos. Environ. 127, 244–254. https://doi.org/10.1016/j.atmosenv.2015.12.015.
Wu, X., Zhang, S., Guo, X., Yang, Z., Liu, J., He, L., Zheng, X., Han, L., Liu, H., Wu, Y., 2019. Assessment of ethanol blended fuels for gasoline vehicles in China: fuel economy, regulated gaseous pollutants and particulate matter. Environ. Pollut. 253, 731–740. https://doi.org/10.1016/j.envpol.2019.07.045.
Xie, K., Li, W., Zhao, W., 2010. Coal chemical industry and its sustainable development in China. Energy, Energy and Its Sustainable Development for China. 35, pp. 4349–4355. https://doi.org/10.1016/j.energy.2009.05.029.
Xiong, C., Wang, N., Zhou, L., Yang, F., Qiu, Y., Chen, J., Han, L., Li, J., 2021. Component characteristics and source apportionment of volatile organic compounds during summer and winter in downtown Chengdu, Southwest China. Atmos. Environ. 258, 118485. https://doi.org/10.1016/j.atmosenv.2021.118485.
Xue, L., Wang, T., Guo, H., Blake, D.R., Tang, J., Zhang, X., Saunders, S.M., Wang, W., 2013. Sources and photochemistry of volatile organic compounds in the remote atmosphere of western China: results from the Mt. Waliguan Observatory. Atmos. Chem. Phys. 13, 8551–8567. https://doi.org/10.5194/acp-13-8551-2013.
Xue, L., Wang, T., Gao, J., Ding, A., Zhou, X., Blake, D.R., Wang, X., Saunders, S.M., Fan, S., Zuo, H., Zhang, Q., Wang, W., 2014. Ground-level ozone in four chinese cities: precursors, regional transport and heterogeneous processes. Atmos. Chem. Phys. 14, 13175–13188. https://doi.org/10.5194/acp-14-13175-2014.
Xue, L., Gu, R., Wang, T., Wang, X., Saunders, S., Blake, D., Louie, P.K.K., Luk, C.W.Y., Simpson, I., Xu, Z., Wang, Z., Gao, Y., Lee, S., Mellouki, A., Wang, W., 2016. Oxidative capacity and radical chemistry in the polluted atmosphere of Hong Kong and Pearl River Delta region: analysis of a severe photochemical smog episode. Atmos. Chem. Phys. 16, 9891–9903. https://doi.org/10.5194/acp-16-9891-2016.
Yang, X., Xue, L., Wang, T., Wang, X., Gao, J., Lee, S., Blake, D.R., Chai, F., Wang, W., 2018. Observations and explicit modeling of summertime carbonyl formation in Beijing: identification of key precursor species and their impact on atmospheric oxidation chemistry. J. Geophys. Res. Atmos. 123, 1426–1440. https://doi.org/10.1002/2017JD027403.
Yin, M., Zhang, X., Li, Y., Fan, K., Li, H., Gao, R., Li, J., 2021. Ambient ozone pollution at a coal chemical industry city in the border of loess plateau and mu Us Desert: characteristics, sensitivity analysis and control strategies. PeerJ 9, e11322. https://doi.org/10.7717/peerj.11322.
Yulin Daily, 2019. Technological and conceptual innovation leads to high-quality development of Yulin Energy and Chemical Base [WWW Document]. URL http://www.sxjiaxian.gov.cn/xwzx/sfyw/36496.htm (accessed 11.28.21).
Zhang, L., Li, H., Wu, Z., Zhang, W., Liu, K., Cheng, X., Zhang, Y., Li, B., Chen, Y., 2020. Characteristics of atmospheric volatile organic compounds in urban area of Beijing: variations, photochemical reactivity and source apportionment. J. Environ. Sci. 95, 190–200. https://doi.org/10.1016/j.jes.2020.03.023 Climate Friendly Air Pollution Control: Sources, Processes, Impacts, and Regulation.
Zhang, Q., Zheng, Y., Tong, D., Shao, M., Wang, S., Zhang, Y., Xu, X., Wang, J., He, H., Liu, W., Ding, Y., Lei, Y., Li, J., Wang, Z., Zhang, X., Wang, Y., Cheng, J., Liu, Y., Shi, Q., Yan, L., Geng, G., Hong, C., Li, M., Liu, F., Zheng, B., Cao, J., Ding, A., Gao, J., Fu, Q., Huo, J., Liu, B., Liu, Z., Yang, F., He, K., Hao, J., 2019b. Drivers of improved PM2.5 air quality in China from 2013 to 2017. PNAS 116, 24463–24469. https://doi.org/10.1073/pnas.1907956116.
Zhang, Y., Yuan, Z., Margni, M., Bulle, C., Hua, H., Jiang, S., Liu, X., 2019a. Intensive carbon dioxide emission of coal chemical industry in China. Appl. Energy 236, 540–550. https://doi.org/10.1016/j.apenergy.2018.12.022.
Zhang, Y., Xue, L., Carter, W.P.L., Pei, C., Chen, T., Mu, J., Wang, Y., Zhang, Q., Wang, W., 2021. Development of ozone reactivity scales for volatile organic compounds in a Chinese megacity. Atmos. Chem. Phys. 21, 11053–11068. https://doi.org/10.5194/acp-21-11053-2021.
Zheng, H., Kong, S., Chen, N., Niu, Z., Zhang, Y., Jiang, S., Yan, Y., Qi, S., 2021. Source apportionment of volatile organic compounds: implications to reactivity, ozone formation, and secondary organic aerosol potential. Atmos. Res. 249, 105344. https://doi.org/10.1016/j.atmosres.2020.105344.